RSC Chemical Biology

ROYAL SOCIETY OF CHEMISTRY

COMMUNICATION

View Article Online
View Journal | View Issue

Cite this: *RSC Chem. Biol.*, 2022, 3, 1096

Received 7th December 2021,
Accepted 1st July 2022

DOI: 10.1039/d1cb00237f

rsc.li/rsc-chembio

Structural guidelines for stabilization of α-helical coiled coils *via* PEG stapling†

Qiang Xiao,[a] Zachary B. Jones,[a] Samantha C. Hatfield,[a] Dallin S. Ashton,[a] Nicholas A. Dalley,[a] Cody D. Dyer,[a] Judah L. Evangelista[b] and Joshua L. Price *[a]

Macrocyclization or stapling is one of the most well-known and generally applicable strategies for enhancing peptide/protein conformational stability and target binding affinity. However, there are limited structure- or sequence-based guidelines for the incorporation of optimal interhelical staples within coiled coils: the location and length of an interhelical staple is either arbitrarily chosen or requires significant optimization. Here we explore the impact of interhelical PEG stapling on the conformational stability and proteolytic resistance of a model disulfide-bound heterodimeric coiled coil. We demonstrate that (1) interhelical PEG staples are more stabilizing when placed farther from an existing disulfide crosslink; (2) *e*/*g*′ staples are more stabilizing than *f*/*b*′ or *b*/*c*′ staples; (3) PEG staples between different positions have different optimal staple lengths; (4) PEG stapling tolerates variation in the structure of the PEG linker and in the mode of conjugation; and (5) the guidelines developed here enable the rational design of a stabilized PEG-stapled HER-2 affibody with enhanced conformational stability and proteolytic resistance.

1. Introduction

Macrocyclization or stapling is one of the most well-known and generally applicable strategies for enhancing peptide/protein conformational stability and target binding affinity.[1–4] Staples preorganize the peptide/protein into a conformation that resembles the folded or bound state by crosslinking two groups that are close to each other in the folded or bound conformation but not in the unfolded or unbound conformation. This covalent constraint prepays part of the energetic cost of folding/binding *via* a combination of entropic and enthalpic effects.

Advances in chemoselective biorthogonal reactions,[5–8] chemical protein synthesis,[9–11] and expression of proteins with unnatural amino acids[12–14] have enabled peptide/protein stapling *via* multiple site-specific strategies. Among the most important of these are thiol alkyl-[15–19] or arylation,[20] olefin metathesis,[21–26] and azide/alkyne cycloaddition.[27–33] We recently showed that stapling *via* olefin metathesis *vs.* the copper-catalyzed azide–alkyne cycloaddition (CuAAC) provide similar increases in the conformational stability of WW, a β-sheet miniprotein derived from the WW domain of the human protein Pin1.[34,35] We observed similar levels of stabilization for staples comprised of discrete polyethylene glycol oligomers (*i.e.*, PEG staples) *vs.* conventional hydrocarbon staples. The most important determinant of PEG-staple-based stabilization in WW is that the two crosslinked groups be far apart in primary sequence but close together in the folded tertiary structure. Presumably this arrangement provides optimal restriction of the conformational freedom of the unfolded ensemble without substantially perturbing the folded state; the resulting destabilization of the unfolded state relative to the folded state provides a more favorable free energy of folding.

Early stapling efforts focused on stabilizing α-helical secondary structure in short peptides.[15,21,22,36–43] Others have expanded this approach more recently to α-helical coiled-coil tertiary/quaternary structure. Coiled-coil primary sequence consists of a seven-residue repeating unit in which non-polar residues occupy the *a*- and *d*-positions within an *abcdefg* heptad; polar and/or charged residue occupy the other positions. Peptides whose sequences follow these patterns are globally amphipathic in an α-helical conformation, with non-polar *a*- and *d*-residues aligned along the same face of the helix. Burial of these *a*- and *d*-residues *via* "knobs-into-holes" packing at the interhelical interface provides the major driving force for coiled-coil self-association. The *e*- and *g*-positions flank the interhelical interface and often engage in complementary electrostatic interactions (*i.e.*, salt bridges). The identify of these *a*-, *d*-, *e*-, and *g*-residues can control

[a] *Department of Chemistry and Biochemistry, Brigham Young University, Provo, Utah 84602, USA. E-mail: jlprice@chem.byu.edu*
[b] *Department of Biochemistry, University of Utah School of Medicine, Salt Lake City, Utah 84112, USA*

† Electronic supplementary information (ESI) available: Experimental methods; compound characterization data, including mass spectra, HPLC chromatograms, and NMR spectra where applicable; CD spectra; global fits of variable temperature CD data; proteolysis assay data. See DOI: https://doi.org/10.1039/d1cb00237f

oligomerization state (dimer, trimer, tetramer, *etc.*); homo- *vs.* hetero-association; and helical orientation (parallel *vs.* antiparallel).[44–47]

Arora and coworkers recently substituted a bis-triazole staple for an interhelical *e*/*e*′ salt bridge within a designed antiparallel coiled-coil heterodimer comprised of nine-residue subunits.[48] They similarly substituted a bis-thioether or bis-triazole staple for an interhelical *e*/*g*′ salt bridge within related parallel coiled-coil heterodimers comprised of 10- or 14-residue subunits.[49] These staples enabled a surprising amount of helicity in such short peptides and the resulting stabilized coiled coils were subsequently useful as scaffolds for rational design of protein–protein interaction inhibitors. Liu, Jiang, and coworkers substituted each of three identical interhelical *e*/*g*′ Glu–Lys salt bridges with an interhelical Glu–Lys isopeptide staple within a trimeric coiled coil derived from the N-terminal domain of HIV-1 gp41.[50] The resulting stapled variant was resistant to proteolysis, aggregation, and thermal denaturation. However, in each of these cases, the precise energetic contribution of the staple to coiled-coil conformational stability was not explored in detail.

Karlström and coworkers used interhelical thioether staples between a chloroacetamide-modified Lys and a nearby Cys to stabilize three proteins that adopt similar monomeric helix-bundle tertiary structures comprised of three α-helices: the albumin binding domain (ABD) of streptococcal protein G,[51] a HER2 affibody (HER2a)[52] and an EGFR affibody (EGFRa).[53] Within each protein, they identified a location where a Cys-Lys staple substantially increases melting temperature (by 5–10 °C). However, Cys-Lys staples at other locations were strongly destabilizing, for reasons that remain unclear. Grossmann and coworkers[54] used a novel tris-electrophile to cross-link non-native Cys residues within the helix-bundle KIX domain. The resulting bicyclic KIX variant bound its partner MLL with similar affinity as its non-stapled counterpart, but had a much higher melting temperature, indicating substantial increase to conformational stability.

Despite these advances, there are limited structure- or sequence-based guidelines for the incorporation of optimal interhelical staples within coiled coils; the location and length of an interhelical staple is either arbitrarily chosen or requires significant optimization.[48] Here we explore the impact of interhelical PEG staples of different lengths and at various solvent-exposed locations on conformational stability and resistance to proteolysis within a model disulfide-bound heterodimeric coiled coil. We demonstrate staple-based stabilization depends strongly on the location of the PEG staple, and that stapling tolerates substantial variations in the structure of the PEG linker with mono- and bis-triazole linkages providing comparable levels of stabilization. Finally, we use the guidelines developed here to generate a stabilized PEG-stapled variant of a HER-2 affibody.

2. Results and discussion

We recently explored the impact of interhelical PEG stapling on the conformational stability of a previously characterized

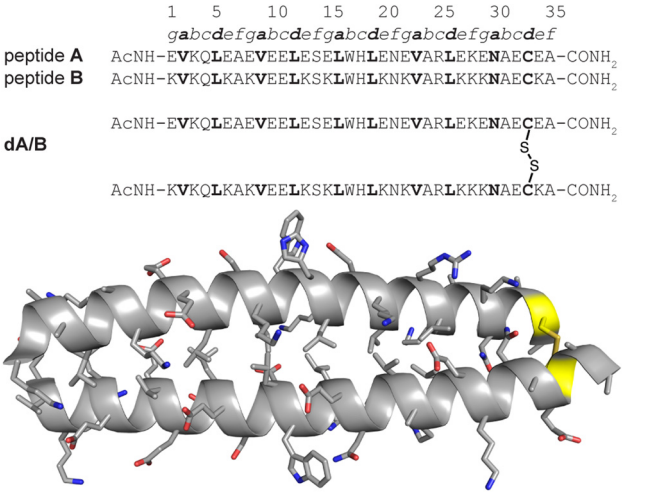

Fig. 1 Sequences of acidic monomer **A**; basic monomer **B**; and disulfide-bound heterodimer **dA/B**. Also shown is the ribbon diagram of **dA/B** (PDB ID: 1KD9) with side chains shown as sticks and Cys33–Cys33′ disulfide highlighted in yellow.

coiled-coil tertiary structure in which acidic peptide A and basic peptide B are connected *via* a disulfide bond to form monomeric two-helix parallel coiled coil **dA/B** (Fig. 1).[55] We prepared non-stapled disulfide-bound variant **d27*e*/29*g*′-z4x** by (1) replacing *e*-position Glu27 in subunit A with **z4**, an Asn derivative in which the side-chain amide nitrogen has been modified with an azide-terminated PEG oligomer comprised of four ethylene oxide units; and (2) replacing *g*-position Lys29′ in subunit B with propargylglycine **x**. (Fig. 2A and B). We then prepared PEG-stapled variant **sd27*e*/29*g*′-z4x** from **d27*e*/29*g*′-z4x** *via* CuAAC, which connects the azide of **z4** to the alkyne of **x** *via* a triazole linkage (Fig. 2C and D).[35] Our approach differs from that of Arora and coworkers[48,49] in the structure of the **z4x** staple and its placement between *e*- and *g*′-positions that are not involved in a salt bridge with each other: in the structure of parent compound **dA/B**, Glu27 is involved in a salt bridge with Lys22′, whereas Lys29′ is involved in a salt bridge with Glu34.

We used the **z4x** staple because modelling suggested that it would readily span the distance between positions 27*e* and 29*g*′ (9.2 Å, based on the distance between side-chain centers of mass at corresponding positions in the crystal structure of **dA/B**; PDB ID 1KD9). Briefly, we generated a model for the **z4x** staple in GaussView 6.0 based on the structure shown in Fig. 2C, but with a single *N*′-acetyl amino acid *N*-methyl amide on either end of the staple. We then optimized this model structure in Gaussian 16 using density functional theory (APFD) calculations with the 6-31G+d,p basis set (see electronic ESI† for details). We used the distance between the β-carbons on either end of the staple as an estimate of the distance that could be comfortably spanned by the **z4x** staple. The calculated length of the **z4x** staple is 18.5 Å (Table 1), which, we hypothesized, would be more than sufficient to span the 9.2 Å between positions 27*e* and 29*g*.

Variable temperature circular dichroism (CD) experiments in 20 mM sodium phosphate buffer (pH 7) with 4 M guanidinium

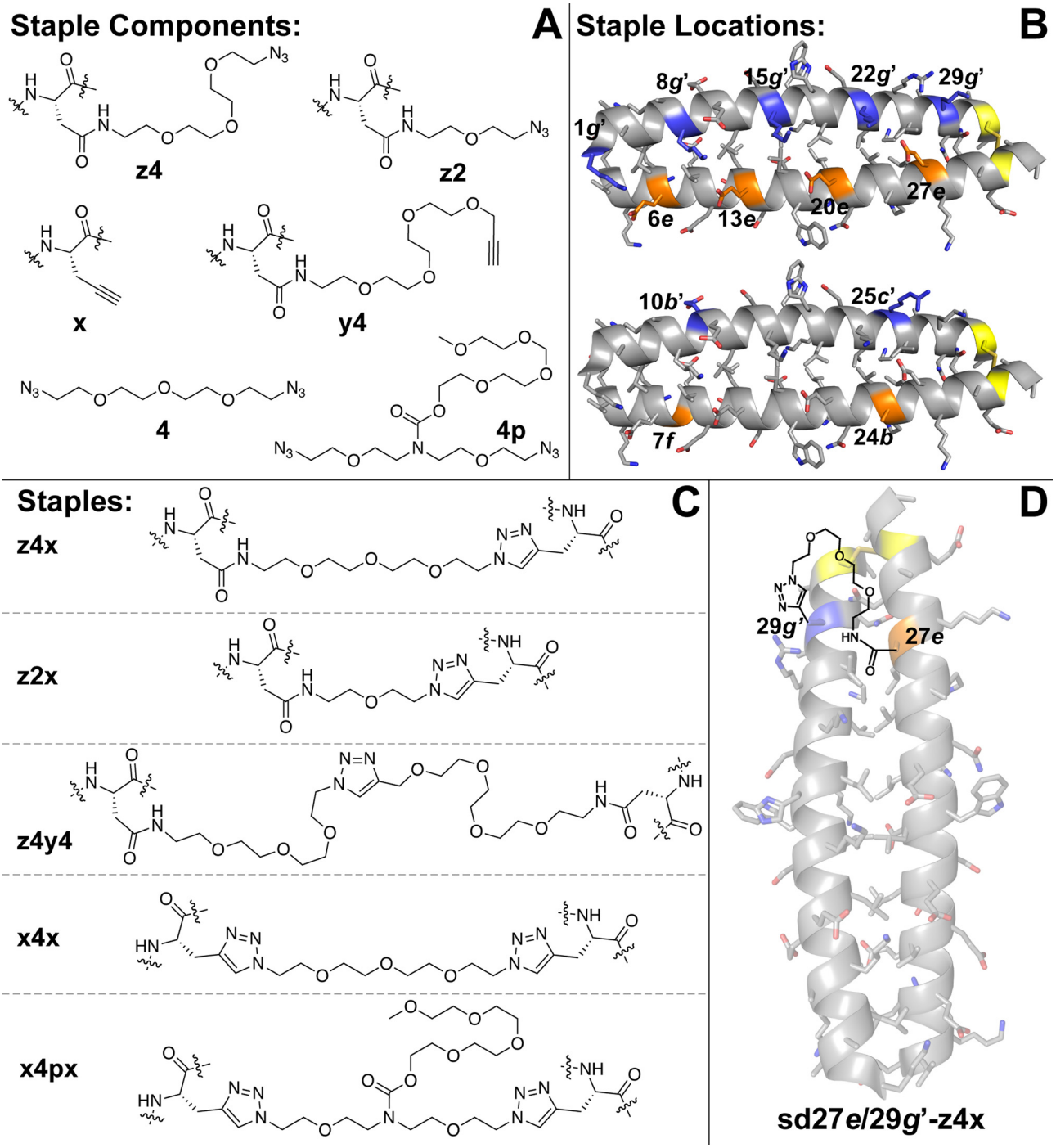

Fig. 2 (A) Structures of staple components, including three Asn derivatives in which the side-chain amide nitrogen has been modified with azide-terminated four- (**z4**) or two-unit PEGs or with an alkyne-terminated four-unit PEG (**y4**). Also shown is propargylglycine (**x**), four-unit bis-azido PEG (**4**) and four-unit bis-azido PEG with branching PEG carbamate (**4p**). (B) Locations within subunits **A** and **B** where we incorporated staple components are highlighted in orange and blue, respectively, on the ribbon diagram of coiled coil **dA/B** (PDB: 1KD9) and are labelled according to their numbered heptad position within the sequence. (C) Structures of staples **z4x**, **z2x**, **z4y4**, **x4x**, and **x4px**, formed from *via* CuAAC from the indicated components. (D) Structure of stapled disulfide-bound variant **sd27*e*/29*g*′-z4x**.

chloride revealed that stapled **sd27*e*/29*g*′-z4x** is -0.65 ± 0.02 kcal mol^{-1} more stable than its non-stapled counterpart due to a favourable entropic effect ($-T\Delta\Delta S = -1.9 \pm 0.06$ kcal mol^{-1}) offset by an unfavourable enthalpic effect ($\Delta\Delta H = 1.3 \pm 0.6$ kcal mol^{-1}). We used denaturant because we were otherwise unable to observe complete or nearly complete thermal unfolding transitions for these and other variants. These observations are consistent with the expectation that stapling limits the conformational freedom of the unfolded ensemble, thereby decreasing the entropic cost of folding.

Table 1 Melting temperatures and folding free energies for non-stapled variants and their PEG-stapled counterparts[a]

Protein	T_m (°C)	Impact of stapling			Distance between staple positions (Å)	Calculated staple length (Å)
		$\Delta\Delta G$ (kcal mol^{-1})	$\Delta\Delta H$ (kcal mol^{-1})	$-T\Delta\Delta S$ (kcal mol^{-1})		
d27*e*/29*g*′-z4x	41.1 ± 0.2					
sd27*e*/29*g*′-z4x	48.2 ± 0.1	−0.65 ± 0.02	1.3 ± 0.6	−1.9 ± 0.6	9.2	18.5
d20*e*/22*g*′-z4x	41.8 ± 0.2					
sd20*e*/22*g*′-z4x	54.3 ± 0.1	−1.09 ± 0.02	1.6 ± 0.6	−2.7 ± 0.6	9.2	18.5
d13*e*/15*g*′-z4x	42.4 ± 0.1					
sd13*e*/15*g*′-z4x	57.7 ± 0.1	−1.33 ± 0.02	2.1 ± 0.5	−3.4 ± 0.5	9.7	18.5
d6*e*/8*g*′-z4x	39.5 ± 0.2					
sd6*e*/8*g*′-z4x	69.1 ± 0.1	−2.53 ± 0.04	−1.9 ± 0.6	−0.7 ± 0.6	10.6	18.5
d27*e*/22*g*′-z4x	43.2 ± 0.1					
sd27*e*/22*g*′-z4x	63.6 ± 0.1	12.01 ± 0.02	−2.7 ± 0.5	0.6 ± 0.5	6.3	18.5
d6*e*/1*g*′-z4x	45.0 ± 0.1					
sd6*e*/1*g*′-z4x	73.7 ± 0.2	−2.30 ± 0.04	1.7 ± 0.6	−4.0 ± 0.6	6.0	18.5
d24*b*/25*c*′-z4x	43.4 ± 0.1					
sd24*b*/25*c*′-z4x	33.0 ± 0.2	0.65 ± 0.02	8.1 ± 0.5	−7.4 ± 0.5	14.3	18.5
d7*f*/10*b*′-z4x	42.6 ± 0.2					
sd7*f*/10*b*′-z4x	51.4 ± 0.3	−0.61 ± 0.03	8.8 ± 0.9	−9.4 ± 0.9	15.6	18.5
d24*b*/25*c*′-z4y4	46.5 ± 0.1					
sd24*b*/25*c*′-z4y4	44.5 ± 0.2	0.17 ± 0.02	0.8 ± 0.6	−0.6 ± 0.6	14.3	28.5
d7*f*/10*b*′-z4y4	43.7 ± 0.2					
sd7*f*/10*b*′-z4y4	54.2 ± 0.2	−0.68 ± 0.01	6.6 ± 0.6	−7.2 ± 0.6	15.6	28.5
d27*e*/29*g*′-z2x	38.8 ± 0.2					
sd27*e*/29*g*′-z2x	33.7 ± 0.1	0.31 ± 0.01	6.1 ± 0.4	−5.8 ± 0.4	9.2	8.1
d27*e*/22*g*′-z2x	43.4 ± 0.1					
sd27*e*/22*g*′-z2x	64.9 ± 0.3	−2.04 ± 0.03	−0.5 ± 0.6	−1.5 ± 0.6	6.3	8.1
d27*e*/29*g*′-xx	39.8 ± 0.2					
sd27*e*/29*g*′-x4x	52.9 ± 0.2	−1.08 ± 0.03	−2.0 ± 0.5	0.9 ± 0.5	9.2	19.3
sd27*e*/29*g*′-x4px	53.4 ± 0.1	−1.21 ± 0.02	−4.1 ± 0.5	2.9 ± 0.5		
affibody a	66.4 ± 0.2					
a8/42-xx	60.9 ± 0.1	0.64 ± 0.02	−2.1 ± 1.1	2.8 ± 1.1	7.4	19.3
sa8/42-x4x	76.1 ± 0.1	−1.09 ± 0.03	3.5 ± 1.3	−4.6 ± 1.3		

[a] Distance between staple positions for each variant were calculated by measuring the distance between the centers of mass of the corresponding side chains in the crystal structure of the parent disulfide-bound coiled-coil heterodimer **dA/B** (PDB ID: 1KD9). Calculated staple length measured from β-carbon to β-carbon within model staple structures (see ESI) optimized in Gaussian 16 using density functional theory APFD and the 6-31G+d,p basis set. $\Delta\Delta G$, $\Delta\Delta H$, and $-T\Delta\Delta S$ values for each variant are given ± std. error in kcal mol^{-1} at the melting temperature of its corresponding non-stapled counterpart at 15 μM protein concentration in 20 mM sodium phosphate buffer (pH 7)+4.0 M GdnHCl, except for affibody **a**, non-stapled **a8/42-xx**, and stapled **sa8/42-x4x**, which were characterized without denaturant.

2.1 Location of staple relative to existing disulfide bridge

The **z4x** PEG staple in variant **sd27*e*/29*g*′-z4x** is close to the Cys33–Cys33′ disulfide in both primary sequence and folded tertiary structure (Fig. 2D). We wondered whether the **z4x** PEG staple might provide superior stabilization between analogous non-salt-bridged *e*- and *g*′-positions farther away from the disulfide (*e.g.*, **20*e*/22*g*′**; **13*e*/15*g*′**; or **6*e*/8*g*′**). To test this hypothesis, we prepared non-stapled disulfide-bound variants **d20*e*/22*g*′-z4x**, **d13*e*/15*g*′-z4x**, and **d6*e*/8*g*′-z4x** (in which **z4** occupies *e*-positions 20, 13, and 6, respectively, whereas **x** occupies *g*-positions 22′, 15′, and 8′, respectively) along with their PEG-stapled counterparts **sd20*e*/22*g*′-z4x**, **sd13*e*/15*g*′-z4x**, and **sd6*e*/8*g*′-z4x**. Staple components, locations, and structures are shown in Fig. 2A–C; see the ESI† for a more detailed representation of the sequence and structure of each variant. In each case, modelling suggested that the **z4x** staple would be more than sufficient for spanning the distance between staple positions (Table 1). As before, we assessed the conformational stability of the PEG-stapled variants relative to their non-stapled counterparts using variable temperature CD experiments in 20 mM sodium phosphate buffer (pH 7) with 4 M guanidinium chloride (Table 1).

The stabilizing impact of the **z4x** PEG staple increases linearly with increasing distance from the Cys33–Cys33 disulfide: **sd20*e*/22*g*′-z4x**, **sd13*e*/15*g*′-z4x**, and **sd6*e*/8*g*′-z4x** are −1.09 ± 0.02, −1.33 ± 0.02, and −2.53 ± 0.04 kcal mol^{-1} more stable, respectively, than their non-stapled counterparts. These observations are congruent with our previous studies[35] in the context of the WW and SH3 domains: a PEG staple yields the greatest energetic benefit when placed between positions close in tertiary structure, but distant from each other in primary sequence or (in this case) from the nearest disulfide crosslink. Consistent with our previous observations for the **z4x** staple at 27*e*/29*g*′, $\Delta\Delta G$ values associated with the **z4x** staples at 20*e*/22*g*′ and at 13*e*/15*g*′ come from favourable entropic terms, which become more favourable with increasing distance from the Cys33–Cys33′ disulfide bond (Table 1). Interestingly, the $\Delta\Delta G$ value for the **z4x** staple at 6*e*/8*g*′ has the smallest favourable entropic term of the series ($-T\Delta\Delta S$ = −0.7 ± 0.6 kcal mol^{-1}), along with a substantial favourable enthalpic term ($\Delta\Delta H$ = −1.9 ± 0.6 kcal mol^{-1}). Interpreting these observations can be difficult due to entropy/enthalpy compensation; however, it is possible that the long-range covalent constraint provided by the **z4x** staple at 6*e*/8*g*′ strengthens existing enthalpically favourable interactions within the coiled coil (*e.g.*, intrahelical *i*-to-*i* + 4 hydrogen bonding; interhelical salt bridges).

2.2 Staples between salt-bridged *vs.* non-salt-bridged *e* and *g* positions

We next wondered whether **z4x** PEG staples (18.5 Å long) might provide similar levels of stabilization at salt-bridged positions 27*e*/22*g*′ or 6*e*/1*g*′ (6.3 and 6.0 Å apart, respectively) as we observed above for non-salt-bridged positions 27*e*/29*g*′ or 6*e*/8*g*′. We explored this possibility by preparing non-stapled variants **d27*e*/22*g*′-z4x** and **d6*e*/1*g*′-z4x** (in which **z4** occupies *e*-positions 27 and 6, whereas **x** occupies *g*-positions 22′ and 1*g*′ respectively), and their stapled counterparts **sd27*e*/22*g*′-z4x** and **sd6*e*/1*g*′-z4x** (Fig. 2B–D). Stapled variant **sd27*e*/22*g*′-z4x** is -1.93 ± 0.02 kcal mol^{-1} more stable than its non-stapled counterpart (Table 1), an effect driven unexpectedly by a favourable enthalpic term ($\Delta\Delta H = -3.4 \pm 0.5$ kcal mol^{-1}) offset by an unfavourable entropic term ($-T\Delta\Delta S = 1.5 \pm 0.5$ kcal mol^{-1}). In contrast, **sd6*e*/1*g*′-z4x** is -2.30 ± 0.04 kcal mol^{-1} more stable than its non-stapled counterpart due to a favourable entropic term ($-T\Delta\Delta S = -4.0 \pm 0.6$ kcal mol^{-1}), offset by an unfavourable enthalpic term ($\Delta\Delta H = 1.7 \pm 0.6$ kcal mol^{-1}). The $\Delta\Delta G$ value for the **z4x** staple at 27*e*/22*g*′ is much more favourable than we observed previously at 27*e*/29*g*′ (-1.93 ± 0.03 kcal mol^{-1} *vs.* -0.65 kcal mol^{-1}). In contrast, the $\Delta\Delta G$ values for the **z4x** staples at 6*e*/1*g*′ *vs.* 6*e*/8*g*′ are similar (-2.30 ± 0.05 kcal mol^{-1} *vs.* -2.53 ± 0.04 kcal mol^{-1}). Placing the **z4x** staple at salt-bridged *vs.* non-salt-bridged *e*- and *g*′-positions appears to matter more at locations closer to the Cys33–Cys33′ disulfide. Alternatively, it is possible that we have reached an upper limit for staple-based stabilization of a disulfide-bound coiled-coil heterodimer.

2.3 Impact of *f*/*b*′ *vs.* *b*/*c*′ PEG Staples

Next, we wondered whether **z4x** staples between other solvent exposed positions (*i.e.*, *b*, *c*, and *f*, Fig. 2B) might provide similar levels of stabilization as we observed for the *e*/*g*′ staples described above. Residues at *b*- and *c*′-positions or at *f*- and *b*′-positions are generally farther apart in space than *e*- and *g*′-positions and are oriented away from instead of toward the interhelical interface. We wondered whether these differences might attenuate the impact of stapling. Accordingly, we prepared variants **d7*f*/10*b*′-z4x** and **d24*b*/25*c*′-z4x** (in which **z4** occupies position 7*f* and position 24*b*, whereas **x** occupies position 10*b*′ and position 25*c*′, respectively) along with their stapled counterparts **sd7*f*/10*b*′-z4x** and **sd24*b*/25*c*′-z4x** (Fig. 2B and C). In both cases, we expected the distance between staple positions (15.6 Å for 7*f*/10*b*′; 14.3 Å for 24*b*/25*c*′) to be near the upper limit of what can be comfortably spanned by the **z4x** staple.

Stapled variant **sd7*f*/10*b*′-z4x** is -0.65 ± 0.03 kcal mol^{-1} more stable than its non-stapled counterpart (Table 1). This is a much smaller level of stabilization than we observed for the **z4x** staples at 6*e*/8*g*′ or 6*e*/1*g*′, which are similarly distant from the disulfide bridge, possibly indicating that **z4x** staples between *f*- and *b*′-positions are less stabilizing than between *e*- and *g*′-positions. Stapled variant **sd24*b*/25*c*′-z4x** is 0.74 ± 0.02 kcal mol^{-1} less stable than its non-stapled counterpart (Table 1), a substantial destabilization that contrasts with the stabilizing impact of the **z4x** staples at 27*e*/29*g*′ or 27*e*/22*g*′, which are similarly distant from the Cys33–Cys33′ disulfide.

2.4 Impact of changes in staple length/structure

We wondered whether poor performance of the **z4x** staples at 7*f*/10*b*′ and at 24*b*/25*c*′ might reflect the increased distances between *f*- and *b*′-positions (15.6 Å) or between *b*- and *c*′-positions (14.3 Å) relative to *e*- and *g*′-positions (6.3–9.2 Å). To test this hypothesis, we prepared variants **d7*f*/10*b*′-z4y4** and **d24*b*/25*c*′-z4y4** (in which **z4** occupies positions 7*f* or 24*b*, whereas **y4** occupies positions 10*b*′ and 25*c*′, respectively) and their stapled counterparts **sd7*f*/10*b*′-z4y4** and **sd24*b*/25*c*′-z4y4** (Fig. 2B and C). The **z4y4** staple has eight ethylene oxide units, whereas the **z4x** staple has only four; indeed, modelling suggests that the **z4y4** staple can comfortably span a much longer distance (28.5 Å) than the **z4x** staple (see ESI†). The impact of the eight-unit **z4y4** staple on the stability of variant **sd7*f*/10*b*′-z4y4** relative to its non-stapled counterpart ($\Delta\Delta G = -0.68 \pm 0.01$ kcal mol^{-1}) is indistinguishable from that of the four-unit **z4x** staple at the same positions. This observation suggests that if a staple is already sufficiently long to span the distance between positions, additional increases in length will not improve staple-based stabilization. In contrast, variant **sd24*b*/25*c*′-z4y4** is 0.17 ± 0.02 kcal mol^{-1} less stable than its non-stapled counterpart, a smaller increment of destabilization than we observed above for the four-unit **z4x** staple at 24*b*/25*c*′. This observation suggests that stapling between some positions is intrinsically destabilizing in a way that increased staple length cannot compensate for. In any case, the **z4y4** staples at 7*f*/10*b* and at 24*b*/25*c*′ provided inferior stabilization relative to the **z4x** staples at the *e*/*g*′-positions described above.

We wondered whether we might enhance the favourable impact of stapling between at 27*e*/29*g*′ or at 27*e*/22*g*′ by truncating the **z4x** staple from four ethylene oxide units to two. Accordingly, we prepared variants **d27*e*/29*g*′-z2x** and **d27*e*/29*g*′-z2x** (in which two-unit azide-terminated Asn derivative **z2** occupies position 27*e*, whereas **x** occupies positions 29*g*′ *vs.* 22*g*′, respectively), and their stapled counterparts **sd27*e*/29*g*′-z2x** and **sd27*e*/29*g*′-z2x** (Fig. 2B and C). The impact of the **z2x** staple at 27*e*/29*g*′ ($\Delta\Delta G = 0.31 \pm 0.01$ kcal mol^{-1}) is much less favourable than that of the **z4x** staple ($\Delta\Delta G = -0.65 \pm 0.02$ kcal mol^{-1}). This effect is driven by an unfavourable enthalpic term ($\Delta\Delta H = 6.1 \pm 0.4$ kcal mol^{-1}), potentially indicating that the two-unit staple disrupts favourable interactions or introduces unfavourable contacts within the coiled coil. Presumably, this reflects the longer distance between 27e/29g′ (9.2 Å) relative to the length of the shorter **z2x** staple (calculated length = 8.1 Å; Table 1). In contrast, the impact of the **z2x** staple at 27*e*/22*g*′ ($\Delta\Delta G = -1.95 \pm 0.04$ kcal mol^{-1}) is indistinguishable from that of the **z4x** staple ($\Delta\Delta G = -1.93 \pm 0.03$ kcal mol^{-1}), an effect driven similarly by enthalpy ($\Delta\Delta H_f = -1.5 \pm 0.6$ kcal mol^{-1}), with a nominally favourable entropic contribution ($-T\Delta\Delta S_f = -0.4 \pm 0.6$ kcal mol^{-1}). This observation is consistent with the shorter distance between 27e/22g′ (6.3 Å) relative to the length of the **z2x** staple (8.1 Å). More generally, it is possible that salt-bridged *e*/*g*′-positions are more tolerant of

shorter staples than are non-salt-bridged *e*/*g*′-positions, due to the closer proximity of the salt-bridged *e*/*g*′-positions.

In preparing the variants above, we incorporated the **z4**, **z2**, **y4**, and **x** staple components at the indicated positions by solid phase peptide synthesis, which becomes progressively less efficient for larger proteins. In contrast, staple component **x** (*i.e.*, propargylglycine) can be incorporated into expressed proteins as a methionine surrogate.[56] We envisioned that stapling of two **x** residues with a bis-azido PEG might be easier to implement in larger proteins than the **z4x** staple. However, we wondered whether such a staple would have a similar impact on coiled-coil conformational stability as we observed for the **z4x** staples. To explore this possibility, we prepared variant **d27*e*/29*g*′-xx** (in which **x** occupies both positions 27*e* and 29*g*′). We then reacted **d27*e*/29*g*′-xx** with four-unit bis-azido PEG **4** (Fig. 2A) *via* CuAAC to give stapled variant **sd27*e*/29*g*′-x4x** (Fig. 2C; calculated staple length = 19.3 Å). Variant **sd27*e*/29*g*′-x4x** is -1.08 ± 0.03 kcal mol^{-1} more stable than its non-stapled counterpart, a modestly larger increment of stabilization than we observed above for the four-unit **z4x** staple between the

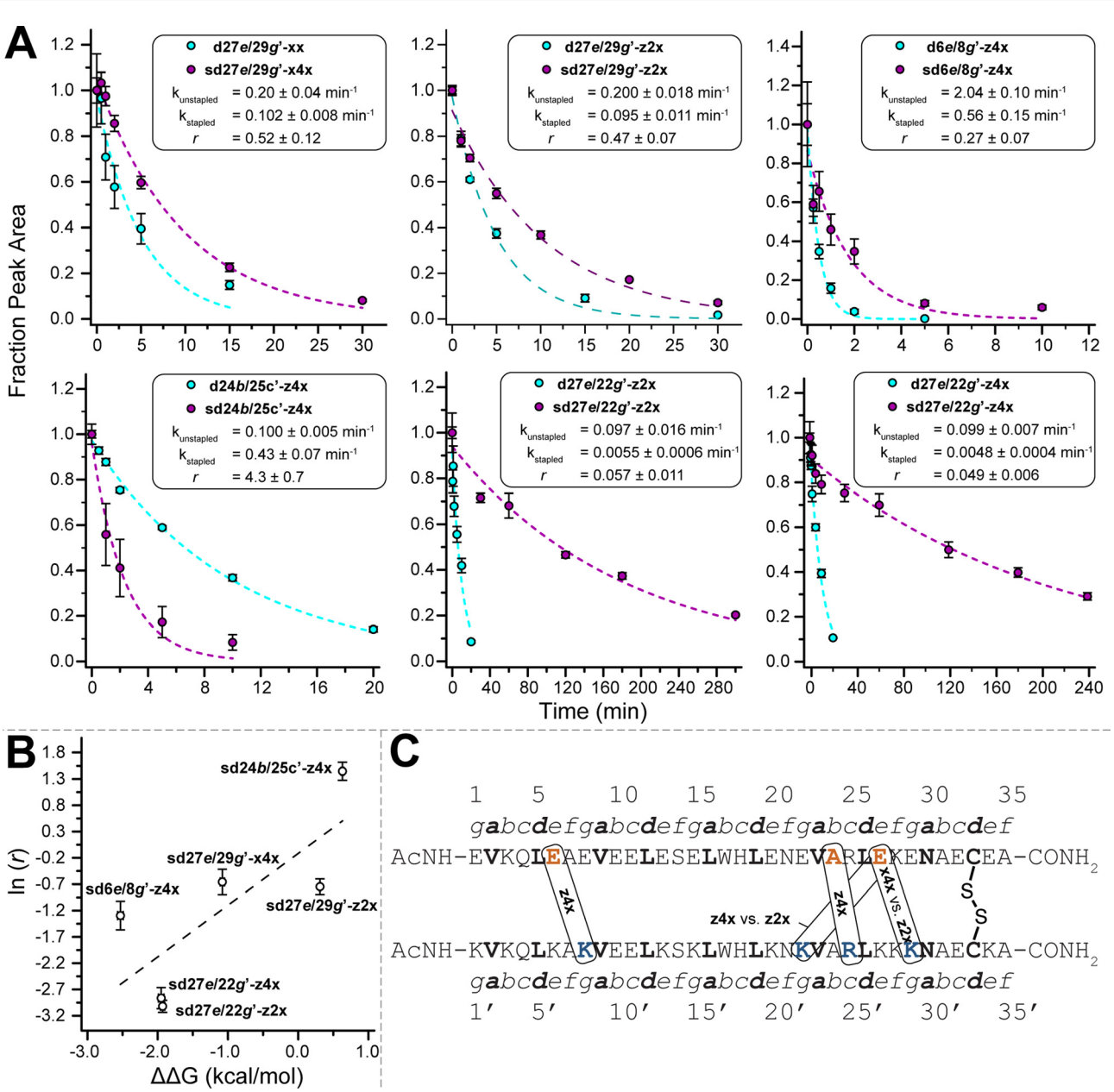

Fig. 3 (A) Proteolysis of selected unstapled and stapled variants by proteinase K (17 μg mL^{-1}) at 15 μM protein concentration in 20 mM sodium phosphate buffer (pH 7) as monitored by HPLC. Data points represent the average of three replicate experiments for unstapled variants (cyan) and for stapled variants (magenta). Coloured dotted lines represent fits of the data for each variant to a mono-exponential decay function, which was used to determine apparent proteolysis rate constants *k* and rate constant ratios *r*. (B) The impact of PEG-stapling on the conformational stability of these variants (ΔΔ*G*) plotted against the natural logarithm of *r*. Black dotted line represents fit of the ln (*r*) *vs.* ΔΔ*G* data to a linear equation. Slope = 0.98 ± 0.40; R^2 = 0.60. (C) Location and identity of the staples investigated here within the disulfide-bound coiled coil.

same positions. Interestingly, the stabilizing impact of the **x4x** staple comes from a favourable enthalpic term, offset by a nominally unfavourable entropic term, suggesting that the precise origins of staple-based stabilization might be different for the four-unit **z4x** *vs.* **x4x** staples.

The modular nature of the **x4x** staple allows us to consider attaching additional groups to the staple, thereby combining the benefits of PEG stapling with additional functionalities (*e.g.*, longer PEG chains; fluorophores, *etc.*). We explored this possibility by preparing branched PEG bis-azide **4p**, in which the central oxygen of the four-unit PEG bis-azide has been replaced with nitrogen, which was subsequently conjugated to an additional linear four-unit PEG *via* a carbamate linkage (Fig. 2A). Stapling of **d27*e*/29*g*′-xx** with PEG bis-azide **4p** *via* CuAAC resulted in variant **sd27*e*/29*g*′-x4px**. Variant **sd27*e*/29*g*′-x4px** is -1.21 ± 0.02 kcal mol^{-1} more stable than non-stapled **d27*e*/29*g*′-xx**. The observation that staples derived from the branched *vs.* linear PEG bis-azides provide similar benefits to conformational stability suggests that one can incorporate additional functional groups within the PEG staple without disrupting staple-based stabilization.

2.5 Impact of PEG stapling on proteolytic resistance

We previously showed that PEG staple-based increases in WW conformational stability are associated with increased levels of protection from proteolysis.[35] We wondered whether this would be true for the PEG-stapled coiled-coil variants described above. We explored this possibility by exposing 15 μM solutions of stapled variants **sd27*e*/29*g*′-z4x**, **sd6*e*/8*g*′-z4x**, **sd27*e*/22*g*′-z4x**, **sd24*b*/25*c*′-z4x**, **sd27*e*/29*g*′-z2x**, **sd27*e*/22*g*′-z2x**, **sd27*e*/29*g*′-x4x**, and their non-stapled counterparts to proteinase K (17 μg mL^{-1}) and monitoring the amount of full-length protein remaining in solution at regular intervals by analytical HPLC. We fit the resulting data for each variant to a monoexponential decay function to obtain apparent proteolysis rate constants k. The results of this analysis are shown in Fig. 3A. All the PEG-stapled variants with improved thermodynamic stability showed enhanced proteolytic resistance, whereas PEG-stapled variants with compromised conformational stability (*e.g.*, **sd24*b*/25*c*′-z4x**) were more vulnerable to proteolysis. For each variant, we calculated a proteolytic resistance factor *r*, which is the ratio between the apparent rate constant *k* for a PEG-stapled variant to that of its non-stapled counterpart. Staples with smaller *r* values provide better protection from proteolysis. We then plotted the natural logarithm of *r* against the corresponding ΔΔ*G* values for each stapled variant relative to its non-stapled counterpart (Fig. 3B). The natural logarithm of *r* varies linearly with ΔΔ*G* (R^2 = 0.60), indicating that staples that better enhance conformational stability generally provide better protection from proteolysis. Interestingly, the **x4x** *vs.* **z2x** staples between positions 27*e* and 29*g*′ provide similar levels of proteolytic resistance even though they have substantially different impacts on conformational stability (**x4x** is stabilizing, whereas **z2x** is not), suggesting that staple location is a more important determinant of proteolytic resistance than is staple length (Fig. 3C).

2.6 Application of PEG-stapling in a HER2 affibody

Finally, we applied the PEG bis-azide stapling strategy to HER2 affibody **a**,[57] which adopts a monomeric helix-bundle conformation comprised of three α-helices. This tertiary structure is closely reminiscent of a trimeric coiled coil, though its sequence does not strictly follow the canonical pattern of the heptad repeat nor does it appear to engage in knobs-into-holes packing. However, positions 8 and 42 (Fig. 4) roughly correspond to the *g*- and *e*-positions we stapled in the **dA/B** coiled coil above; they are solvent exposed; and are similarly close to each other in tertiary structure (~7.4 Å between side-chain centers of mass) but are far apart in primary sequence. We prepared non-stapled affibody variant **a8/42-xx** (in which **x** occupies both positions 8 and 42). We then reacted **a8/42-xx** with four-unit PEG bis-azide **4** to give stapled variant **sa8/42-x4x**. We also prepared the unmodified parent HER2 affibody **a**, in which Glu and Ala occupy positions 8 and 42, respectively. PEG-stapled affibody **sa8/42-x4x** is -1.09 ± 0.02 kcal mol^{-1} more stable than the native affibody **a** and is -1.60 ± 0.03 kcal mol^{-1}

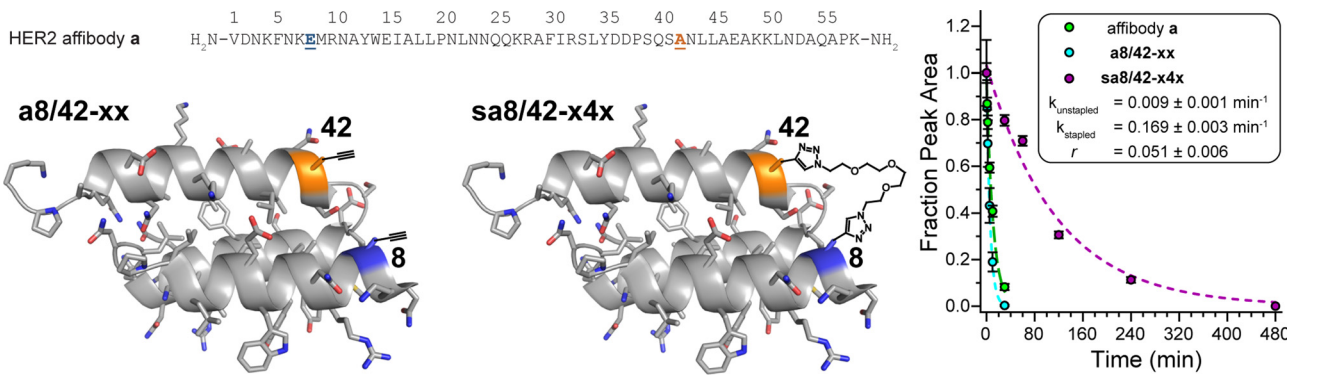

Fig. 4 Sequence of HER2 affibody **a**. Also shown are structures of variant **a8/42-xx** and its stapled counterpart **sa8/42-x4x** drawn on the ribbon diagrams of parent affibody **a** (PDB: 3MZW); locations where we incorporated staple component **x** or staple **x4x** are highlighted in orange and blue and are labelled according to their numbered heptad positions within the sequence. Also shown are proteolysis data for affibody **a** (green), unstapled variant **a8/42-xx** (cyan), and stapled **sa8/42-x4x** (magenta) in proteinase K (17 mg mL^{-1}) at 15 μM protein concentration in 20 mM sodium phosphate buffer (pH 7) as monitored by HPLC. Data points represent the average of three replicate experiments. Colored dotted lines represent fits of the data for each variant to a mono-exponential decay function, which we used to calculate apparent proteolysis rate constants *k* and rate constant ratio *r*.

more stable than non-stapled **a8/42-xx** (chemical denaturant was unnecessary for variable temperature CD experiments on the affibody and its derivatives). Proteolysis assays analogous to those described above indicate that stapled **sa8/42-x4x** is nine-times more resistant to proteolysis than parent affibody **a** and seventeen-times more resistant to proteolysis than non-stapled **a8/42-xx** (Fig. 4). Fluorescence polarization direct binding assays reveal that the unstapled affibody variant binds the extracellular domain of the HER2 protein with a dissociation constant (K_d) of 0.38 ± 0.05 nM, whereas the K_d for the stapled variant (0.69 ± 0.10 nM) is only slightly higher than that of its unstapled counterpart (see ESI†), suggesting that the enhanced proteolytic resistance conferred by PEG-stapling is not accompanied by dramatic decreases in binding affinity.

3. Conclusions

Here we have explored the impact of PEG stapling on the conformational and proteolytic stability of a disulfide-bonded α-helical coiled-coil heterodimer. Our observations provide important insights into the structural determinants of staple-based stabilization within coiled coils. Interhelical PEG staples (1) are more stabilizing when placed farther from an existing disulfide crosslink; (2) are more stabilizing between salt-bridged *e*- and *g*′-positions than between non-salt-bridged *e*- and *g*′-positions; (3) are more stabilizing between *e*- and *g*-positions generally than between *f*- and *b*′- or *b*- and *c*′-positions; and (4) appear to be most stabilizing when the calculated staple length exceeds the distance between staple positions by a reasonable margin. We also found that the PEG-staple is tolerant of additional functional groups within the staple: in fact, an appended branching PEG increased the stabilizing impact of the staple by a modest amount. Finally, we demonstrated that stapling does not significantly compromise binding affinity in a HER2 affibody, whilst conferring substantial proteolytic resistance. Our observations now enable the rational design of PEG-stapled α-helical peptide/protein tertiary structures with predictably enhanced conformational stability and proteolytic resistance.

Conflicts of interest

There are no conflicts to declare.

Acknowledgements

This work was supported by NIH Grant number 2R15GM116055-02. The authors acknowledge Profs. Michael S. Kay and Debra M. Eckert at the University of Utah for assistance with fluorescence polarization experiments.

References

1 D. J. Cram, *Angew. Chem., Int. Ed. Engl.*, 1986, **25**, 1039–1057.
2 J. M. Lehn, *Angew. Chem., Int. Ed. Engl.*, 1988, **27**, 89–112.
3 C. J. Pedersen, *Angew. Chem., Int. Ed. Engl.*, 1988, **27**, 1021–1027.
4 V. J. Hruby, *Life Sci.*, 1982, **31**, 189–199.
5 H. Y. Chow, Y. Zhang, E. Matheson and X. Li, *Chem. Rev.*, 2019, **119**, 9971–10001.
6 T. K. Tiefenbrunn and P. E. Dawson, *Biopolymers*, 2010, **94**, 95–106.
7 C. P. R. Hackenberger and D. Schwarzer, *Angew. Chem., Int. Ed.*, 2008, **47**, 10030–10074.
8 J. N. deGruyter, L. R. Malins and P. S. Baran, *Biochemistry*, 2017, **56**, 3863–3873.
9 D. Schumacher and C. P. R. Hackenberger, *Curr. Opin. Chem. Biol.*, 2014, **22**, 62–69.
10 J. M. Chalker, *Chem. Biol. Drug Des.*, 2013, **81**, 122–135.
11 P. E. Dawson, T. W. Muir, I. Clarklewis and S. B. H. Kent, *Science*, 1994, **266**, 776–779.
12 B. C. Bundy and J. R. Swartz, *Bioconjugate Chem.*, 2010, **21**, 255–263.
13 J. T. Ngo and D. A. Tirrell, *Acc. Chem. Res.*, 2011, **44**, 677–685.
14 L. Wang, A. Brock, B. Herberich and P. G. Schultz, *Science*, 2001, **292**, 498–500.
15 F. M. Brunel and P. E. Dawson, *Chem. Commun.*, 2005, 2552–2554, DOI: **10.1039/B419015G**.
16 F. Zhang, O. Sadovski, S. J. Xin and G. A. Woolley, *J. Am. Chem. Soc.*, 2007, **129**, 14154–14155.
17 N. Bionda, A. L. Cryan and R. Fasan, *ACS Chem. Biol.*, 2014, **9**, 2008–2013.
18 L. Peraro, T. R. Siegert and J. A. Kritzer, in *Peptide, Protein and Enzyme Design*, ed. V. L. Pecoraro, 2016, vol. 580, pp. 303–332.
19 E. J. Moore, D. Zorine, W. A. Hansen, S. D. Khare and R. Fasan, *Proc. Natl. Acad. Sci. U. S. A.*, 2017, **114**, 12472–12477.
20 A. J. Rojas, C. Zhang, E. V. Vinogradova, N. H. Buchwald, J. Reilly, B. L. Pentelute and S. L. Buchwald, *Chem. Sci.*, 2017, **8**, 4257–4263.
21 H. E. Blackwell and R. H. Grubbs, *Angew. Chem., Int. Ed.*, 1998, **37**, 3281–3284.
22 C. E. Schafmeister, J. Po and G. L. Verdine, *J. Am. Chem. Soc.*, 2000, **122**, 5891–5892.
23 L. D. Walensky, A. L. Kung, I. Escher, T. J. Malia, S. Barbuto, R. D. Wright, G. Wagner, G. L. Verdine and S. J. Korsmeyer, *Science*, 2004, **305**, 1466–1470.
24 R. N. Chapman, G. Dimartino and P. S. Arora, *J. Am. Chem. Soc.*, 2004, **126**, 12252–12253.
25 A. Patgiri, A. L. Jochim and P. S. Arora, *Acc. Chem. Res.*, 2008, **41**, 1289–1300.
26 G. L. Verdine and G. J. Hilinski, *Methods Enzymol.*, 2012, **503**, 3–33.
27 M. Roice, I. Johannsen and M. Meldal, *QSAR Comb. Sci.*, 2004, **23**, 662–673.
28 S. Cantel, A. Le Chevalier Isaad, M. Scrima, J. J. Levy, R. D. DiMarchi, P. Rovero, J. A. Halperin, A. M. D'Ursi, A. M. Papini and M. Chorev, *J. Org. Chem.*, 2008, **73**, 5663–5674.
29 Y. H. Lau, Y. T. Wu, P. de Andrade, W. R. J. D. Galloway and D. R. Spring, *Nat. Protoc.*, 2015, **10**, 585–594.
30 C. M. Haney, H. M. Werner, J. J. McKay and W. S. Horne, *Org. Biomol. Chem.*, 2016, **14**, 5768–5773.

31 P. T. Tran, C. O. Larsen, T. Rondbjerg, M. De Foresta, M. B. A. Kunze, A. Marek, J. H. Loper, L. E. Boyhus, A. Knuhtsen, K. Lindorff-Larsen and D. S. Pedersen, *Chem. – Eur. J.*, 2017, **23**, 3490–3495.
32 M. Scrima, A. Le Chevalier-Isaad, P. Rovero, A. M. Papini, M. Chorev and A. M. D'Ursi, *Eur. J. Org. Chem.*, 2010, 446–457.
33 S. A. Kawamoto, A. Coleska, X. Ran, H. Yi, C.-Y. Yang and S. Wang, *J. Med. Chem.*, 2012, **55**, 1137–1146.
34 Q. Xiao, N. A. Becar, N. P. Brown, M. S. Smith, K. L. Stern, S. R. E. Draper, K. P. Thompson and J. L. Price, *Org. Biomol. Chem.*, 2018, **16**, 8933–8939.
35 Q. Xiao, D. S. Ashton, Z. B. Jones, K. P. Thompson and J. L. Price, *RSC Chem. Biol.*, 2020, **1**, 273–280.
36 G. Osapay and J. W. Taylor, *J. Am. Chem. Soc.*, 1992, **114**, 6966–6973.
37 M. Chorev, E. Roubini, R. L. Mckee, S. W. Gibbons, M. E. Goldman, M. P. Caulfield and M. Rosenblatt, *Biochemistry*, 1991, **30**, 5968–5974.
38 D. Y. Jackson, D. S. King, J. Chmielewski, S. Singh and P. G. Schultz, *J. Am. Chem. Soc.*, 1991, **113**, 9391–9392.
39 A. M. Leduc, J. O. Trent, J. L. Wittliff, K. S. Bramlett, S. L. Briggs, N. Y. Chirgadze, Y. Wang, T. P. Burris and A. F. Spatola, *Proc. Natl. Acad. Sci. U. S. A.*, 2003, **100**, 11273–11278.
40 F. M. Brunel, M. B. Zwick, R. M. F. Cardoso, J. D. Nelson, I. A. Wilson, D. R. Burton and P. E. Dawson, *J. Virol.*, 2006, **80**, 1680–1687.
41 J. R. Kumita, O. S. Smart and G. A. Woolley, *Proc. Natl. Acad. Sci. U. S. A.*, 2000, **97**, 3803–3808.
42 Y. Wang and D. H.-C. Chou, *Angew. Chem., Int. Ed.*, 2015, **54**, 10931–10934.
43 H. Jo, N. Meinhardt, Y. Wu, S. Kulkarni, X. Hu, K. E. Low, P. L. Davies, W. F. DeGrado and D. C. Greenbaum, *J. Am. Chem. Soc.*, 2012, **134**, 17704–17713.
44 F. H. C. Crick, *Acta Crystallogr.*, 1953, **6**, 689–697.
45 P. Burkhard, J. Stetefeld and S. V. Strelkov, *Trends Cell Biol.*, 2001, **11**, 82–88.
46 D. N. Woolfson, *Adv. Protein Chem.*, 2005, **70**, 79–112.
47 A. N. Lupas and M. Gruber, *Adv. Protein Chem.*, 2005, **70**, 37–78.
48 M. G. Wuo, A. B. Mahon and P. S. Arora, *J. Am. Chem. Soc.*, 2015, **137**, 11618–11621.
49 M. G. Wuo, S. Hong, A. Singh and P. S. Arora, *J. Am. Chem. Soc.*, 2018, **140**, 16284–16290.
50 C. Wang, X. Li, F. Yu, L. Lu, X. Jiang, X. Xu, H. Wang, W. Lai, T. Zhang, Z. Zhang, L. Ye, S. Jiang and K. Liu, *Sci. Rep.*, 2016, **6**, 32161.
51 J. Lindgren and A. Eriksson Karlström, *ChemBioChem*, 2014, **15**, 2132–2138.
52 T. Ekblad, V. Tolmachev, A. Orlova, C. Lendel, L. Abrahmsén and A. E. Karlström, *Pept. Sci.*, 2009, **92**, 116–123.
53 A. Nilsson, J. Lindgren and A. Eriksson Karlström, *ChemBioChem*, 2017, **18**, 2056–2062.
54 M. Pelay-Gimeno, T. Bange, S. Hennig and T. N. Grossmann, *Angew. Chem., Int. Ed.*, 2018, **57**, 11164–11170.
55 A. E. Keating, V. N. Malashkevich, B. Tidor and P. S. Kim, *Proc. Natl. Acad. Sci. U. S. A.*, 2001, **98**, 14825–14830.
56 F. Truong, T. H. Yoo, T. J. Lampo and D. A. Tirrell, *J. Am. Chem. Soc.*, 2012, **134**, 8551–8556.
57 C. Eigenbrot, M. Ultsch, A. Dubnovitsky, L. Abrahmsén and T. Härd, *Proc. Natl. Acad. Sci. U. S. A.*, 2010, **107**, 15039–15044.